09,04

Paramagnetic resonance of Fe^{3+} and Cu^{2+} centers in yttrium orthosilicate doped with iron

© M.Yu. Artyomov[1], A.P. Potapov[1], K.A. Soubbotin[2,3], V.A. Vazhenin[1], A.I. Titov[2], A.V. Fokin[1], S.K. Pavlov[2,3], O.N. Lis[2]

[1] Ural Federal University (Institute of Natural Sciences and Mathematics), Yekaterinburg, Russia
[2] Prokhorov Institute of General Physics, Russian Academy of Sciences, Moscow, Russia
[3] Mendeleev University of Chemical Technology, Moscow, Russia

E-mail: vladimir.vazhenin@urfu.ru

Received February 15, 2024
Revised February 15, 2024
Accepted February 16, 2024

Two Fe^{3+} centers, as well as the spectrum of an uncontrolled Cu^{2+} impurity, were studied using paramagnetic resonance in a specially grown $Y_2SiO_5:Fe$ crystal. The parameters of spin Hamiltonians are determined both in laboratory and local (with diagonal second-rank fine structure tensor or hyperfine interaction tensor **A**) coordinate systems. The localization of Fe^{3+}, Cr^{3+}, Gd^{3+} and Cu^{2+} centers in yttrium and scandium silicates is discussed.

Keywords: orthosilicates, impurity ions, paramagnetic resonance.

DOI: 10.61011/PSS.2024.03.57944.27

1. Introduction

The studies [1,2] discuss whether development of materials for quantum electronics, quantum cybernetics, scintillators and other applications can use results of electron paramagnetic resonance (EPR) that allows determining concentrations and oxidation states of paramagnetic uncontrolled impurities when the scale of their concentrations in a sample is about several ppm or even less. Implementation of this activity with yttrium and scandium orthosilicates requires valid information about spectra of the EPR centers of transition and rare-earth impurity elements in these crystals, which are actual for the above-said applications.

Chromium doped Y_2SiO_5 crystal is studied as an active medium for solid-state infrared lasers [3] and as a saturable absorber [4]. The Sc_2SiO_5 single-crystals attract attention of researchers due to their applicability in the solid-state lasers at rare-earths ions.

As a result of EPR investigation of the $Y_2SiO_5:Cr$ crystals, the authors [5] have mistakenly concluded that the spectrum observed by them in the X-range was due to the Cr^{4+} ions with the electron spin $S = 1$, localized in the tetrahedral silicon site. However, the studies [6,7] have convincingly shown that the EPR spectrum in this range actually belongs to the Cr^{3+} ion having the spin $S = 3/2$ and located in one of the two physically non-equivalent Y^{3+} positions. At the same time, this crystal has been studied using a method of polarized optical absorption spectroscopy [8] to show dominance of the absorption bands of the Cr^{4+} ions localized in the silicon positions.

The EPR spectrum of this center has been found and reliably identified only later, in the study [9] that investigated the Y_2SiO_5 crystal doped with the odd ^{53}Cr isotope with a non-zero nuclear spin ($I = 3/2$). The studies were firstly performed on a broadband EPR spectrometer and, then, on the Q-range spectrometer within a wide range of the magnetic fields. Besides, a decrease in repulsion of the energy levels of the Cr^{4+} centers in orientations of the magnetic field near the principal axis of the local coordinate system made it possible to detect the spectrum of this center in the X-range as well. The concentration of the Cr^{4+} has turned out to be only in three times smaller than the number of the Cr^{3+} ions [9]. The EPR studies of the $Sc_2SiO_5:Cr$ crystal [6,10] that was isostructural to yttrium silicate have shown that this crystal contains two Cr^{3+} centers localized in the two physically non-equivalent scandium positions.

When investigating the $Y_2SiO_5:^{53}Cr$ crystal, the study [8] has found and described the EPR spectrum of the second Cr^{3+} center localized in the second yttrium position. This spectrum demonstrates a hyperfine structure and has intensity two orders of magnitude less than the Cr^{3+} spectrum in the $Y_2SiO_5:Cr$ crystal, which is studied in [6,10]. Moreover, multiple narrow and weak (in comparison with the intense Cr^{3+} lines) EPR signals have been found in the Y_2SiO_5 spectra that were not identified at that stage. It was assumed that these signals belong to the uncontrolled Gd^{3+} impurity ions.

Then, using the EPR method, the authors [10–13] have studied the Cr^{3+}, Gd^{3+}, Fe^{3+} centers that were also localized in the positions of the quasi-rare-earth ions in the yttrium and scandium silicate crystals.

The present study is the EPR study of the Fe^{3+} centers in a specially grown Y_2SiO_5 : Fe crystal, as well as of the spectrum of the uncontrolled Cu^{2+} impurity which was found in the same crystal, their structure and localization in the crystal were established. Besides, taking into account the obtained results, the study also discusses issues of localization of the previously studied centers of iron, chromium and gadolinium in yttrium and scandium orthosilicate crystals.

2. Samples and measurement procedure

For measurements, we have grown a Y_2SiO_5 single-crystal doped with iron with the nominal (charge) concentration of 1.7 at.%. The crystal was grown by Czochralski method at a „Crystal-2" plant (USSR) from iridium crucible with an internal diameter and a height of 30 mm) in a slightly-oxidizing atmosphere ($N_2 + 1.35$ vol.% O_2). The actual concentration of oxygen in the growth atmosphere was measured by the analyzer AKPM-01 (Alfa-Bassens, Russia). „Seeding" was carried out onto an iridium wire. At the nominal growth state, the rates of pulling and rotations were 1 mm/h and 6 rpm, respectively.

The charge for growth was prepared from especially pure reagents Y_2O_3 (TU 05-32-69, REAKhIM, USSR), SiO_2 (W30, Wacker Chemie AG, Germany) and Fe_2O_3 (TU 6-09-1418-78, REAKhIM, USSR) by weighing them on electronic analytical balance after pre-drying. The reagent mixture was thoroughly mixed by means of a multi-rotator RS-60 (BioSan, Latvia) for 2 h and pressed into tablets, which were then calcined in air at the temperature of 700°C for 5 h in an EKPS-10 furnace (Smolensk SKTB SPU, Russia).

After completion of the growth process and detachment of the grown crystal from a melt surface, it was cooled to the room temperature at the rate of 8°C/h in order to avoid crystal cracking. The grown crystal was almost colorless, but not totally uniformly dyed: the top part has barely detectable bluish shade, whereas the bottom part was slightly yellowish. After growing, the crystal was additionally annealed in air in the muffle furnace at the temperature of 900°C for 3 weeks in order to relieve thermal stresses and restore of the oxygen stoichiometry. After annealing, the crystal obtained uniform barely noticeable yellowish tint.

The crystal was oriented in respect to optical indicatrix axes using crystallooptic methods by means of a polarization optical microscope „Biomed-5" (China). The orientation error did not exceed 1°. After orientation, the samples were cut in the form of cubes with a side of 6 mm for EPR measurements. The cube faces were perpendicular to the optical indicatrix axes.

The orientation behavior of the EPR spectra of the Y_2SiO_5 : Fe sample was measured at room temperature on an X-range EMX Plus Bruker spectrometer in fields up to 1.41 T. The sample in a spectrometer resonant cavity was attached to a holder that is secured on the rod of the standard automatic goniometer and designed to rotate around the axis perpendicular to the rod. The sample was cut out of an oriented cube and sized as $6 \times 6 \times 1\,mm^3$ with a **b** crystallographic axis lying in a quadrate plane and orthogonal to its side.

3. Fe^{3+} centers

Figure 1 shows the EPR spectrum of the Y_2SiO_5 crystal doped with iron in orientation of the magnetic field $\mathbf{B} \parallel \mathbf{b}$. The spectrum has wide intense signals of a accidental impurity of the Gd^{3+} ions from the Gd1 and Gd2 centers investigated in the study [12]. The positions and the intensity ratio of these centers are similar to the spectrum of Figure 4 in [12].

The Y_2SiO_5 : Fe sample exhibits two non-equivalent centers of trivalent iron, which are similar to the previously-described iron centers in scandium silicate [2]. Hereinafter they are referred to as Fe^{3+}-1 and Fe^{3+}-2. The peak intensities of the first derivatives of the absorption spectrum of only two transitions of the Fe^{3+}-1 center of Figure 1 are comparable to those for the Gd1 and Gd2 signals. But, due to a big width, their integral intensities exceed the similar values for Gd1 and Gd2 in dozens of times. The ratio of the concentrations of the Fe^{3+}-1/Fe^{3+}-2 centers in the Y_2SiO_5 : Fe samples, as obtained taking into account the transition probabilities, is about 500 : 1, whereas the number of the Fe-1 and Fe-2 centers in the previously studied Sc_2SiO_5 crystal is quite comparable (Table 1, 2).

Taking into account the probabilities of the Gd1 and Gd2 transitions using the integral intensities has shown that the concentration of Gd1 and Gd2 in Y_2SiO_5 were almost the same. The integral intensity evaluated as a product of the peak intensity of the first derivative and a square of the line width has provided a value that is close to the result of double integration.

The structure of the Y_2SiO_5 crystals according to the studies [14–16] belongs to a monoclinic crystal system, the space group $C2/c$ (C_{2h}^6). All the atoms in the structure have a triclinic local symmetry 1 (C_1): silicon is in a distorted oxygen tetrahedron, the Y^{3+} ions occupy two non-equivalent positions with coordination numbers 6 ($M1$) and 7 ($M2$). Each atomic position is multiplied by the unit cell symmetry elements (inversion center and axis $C_2 \parallel \mathbf{b}$) up to four. In this regard, if the paramagnetic ion is localized in any of the three positions ($M1$, $M2$, Si), two magnetically non-equivalent spectra will be observed in EPR. And when the **B** magnetic field induction vector is in the **ac** lattice plane or parallel to the **b** crystallographic axis, then these two spectra become equivalent.

The orientation behavior of the positions of the EPR transitions was measured by rotation of the magnetic field in the **ac** plane (the azimuth dependence) and from $\mathbf{B} \parallel \mathbf{b}$ to **B** in the **ac** plane (the polar dependence). The orthogonal laboratory coordinate system **xyz** [12] was used. In this system $\mathbf{z} \parallel \mathbf{b}$, and the **x** and **y** axes are lying in the **ac** plane.

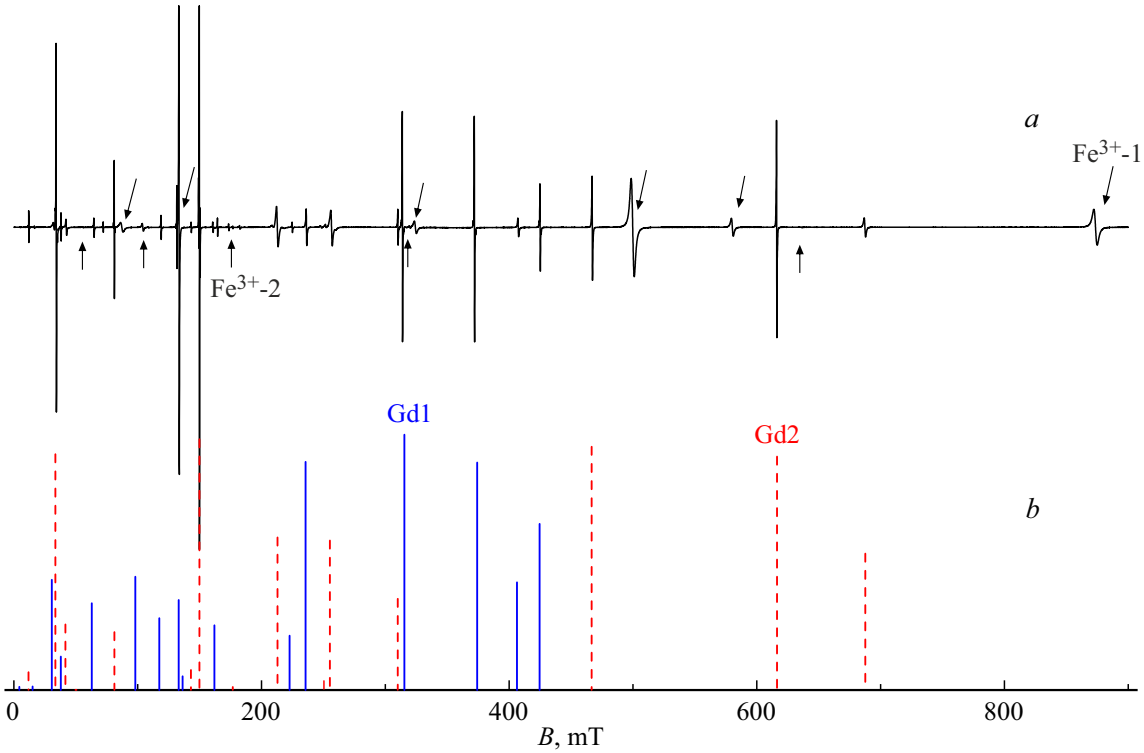

Figure 1. *a* — the EPR spectrum of Y_2SiO_5 with the iron impurity in the orientation **B** || **b** (**B** is the magnetic field) at the room temperature on the frequency of 9813 MHz, the upper arrows indicate the transitions of Fe^{3+}-1, lower arrows — the signals of Fe^{3+}-2. *b* — the calculated positions and the integral intensities of the centers of Gd1 (the blue solid lines) and Gd2 (the red dashed lines).

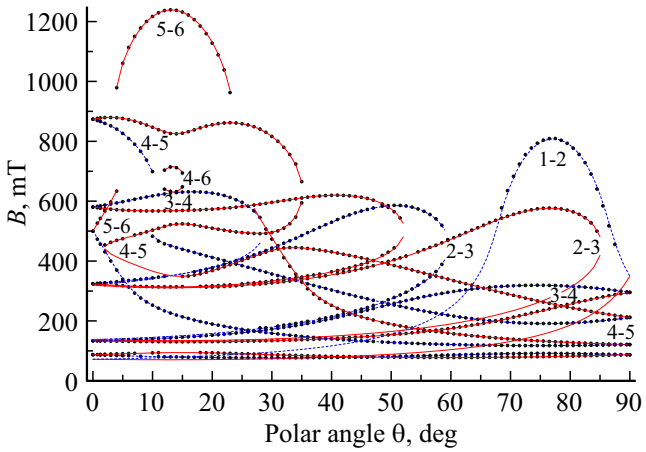

Figure 2. Polar dependences of the positions of the transitions of the Fe^{3+}-1 centers at $\varphi = 23°$ on the frequency of 9812 MHz. The variously-colored and -typed calculated curves (solid, dash) correspond to sets of parameters of the spin Hamiltonian with the opposite signs of b_{nm}, c_{nm} with the odd m and describe the behavior of the two centers that are coupled by the C_2 || **b** rotation.

The angle between the **x** and **a*** axes (**a*** — projection of the **a** axis to the plane that is orthogonal to the **c** axis) is about 6.5° [12].

The polar angular dependences of the experimental positions of the signals of the Fe^{3+}-1, Fe^{3+}-2 centers are shown on Figure 2–3, whereas the azimuth dependences are shown on Figure 4–5. When measuring the azimuth dependences, slight splitting of the signals of the iron centers due to deviation of the magnetic field from the **ac** plane. At the same time, more substantial splitting was detected for the signals of the Gd2 centers (the transitions 6–7

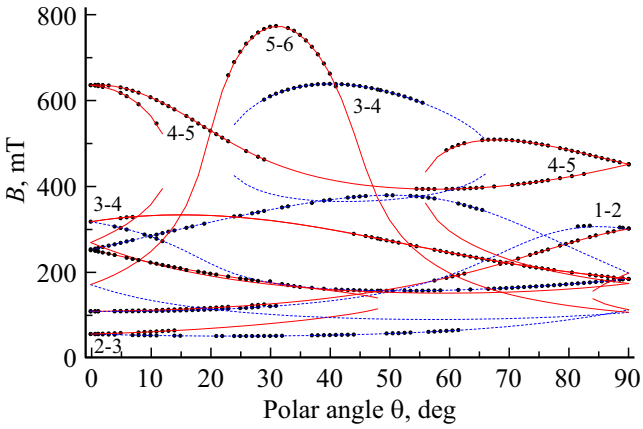

Figure 3. Polar dependences of the positions of the transitions of the Fe^{3+}-2 centers at $\varphi = 23°$ on the frequency of 9812 MHz. The variously-colored and -typed calculated curves (solid, dash) correspond to sets of parameters of the spin Hamiltonian with the opposite signs of b_{nm}, c_{nm} with the odd m and describe the behavior of the two centers that are coupled by the C_2 || **b** rotation.

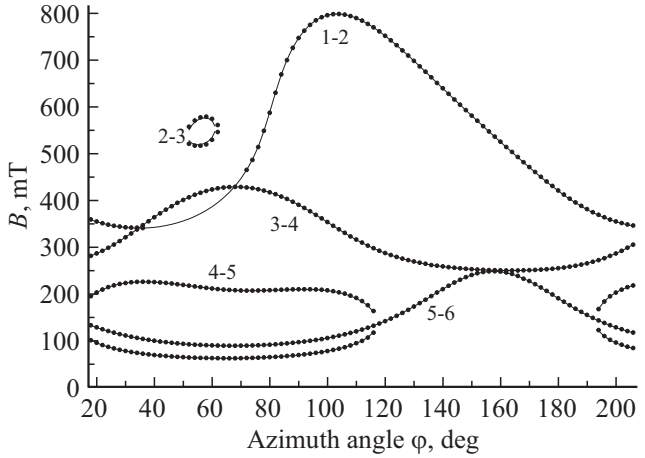

Figure 4. Orientation behavior of the positions of transitions of the Fe^{3+}-1 center in the azimuth plane on the frequency of 9812 MHz. The dots — the experiment, the curves — calculation with the parameters of Table 1 at **z** || **b**.

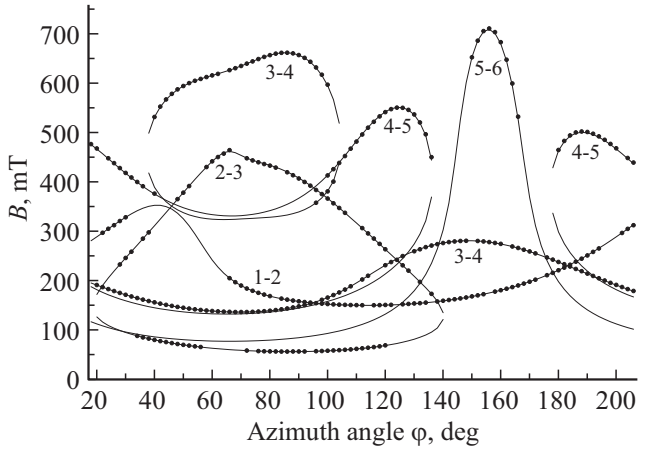

Figure 5. Orientation behavior of the positions of transitions of the Fe^{3+}-2 center in the azimuth plane on the frequency of 9812 MHz. The dots — the experiment, the curves — calculation with the parameters of Table 1 at **z** || **b**.

and 7−8) [12], which were also observed in this sample. The strongest effect was observed near $\varphi = 20°$. The polar dependence of these transitions with the parameters [12] at such φ has been calculated to show that the deviation of **B** from the **ac** plane was about 0.15°.

The Fe^{3+} spectra have been described by means of the spin Hamiltonian (SH) of the triclinic symmetry with the electron spin $S = 5/2$ [17]:

$$H_{sp} = \beta(\mathbf{BgS}) + 1/3\sum_m (b_{2m}O_{2m} + c_{2m}\Omega_{2m})$$

$$+ 1/60\sum_m (b_{4m}O_{4m} + c_{4m}\Omega_{4m}),$$

where **g** — the **g**-tensor, β — the Bohr magneton, O_{nm}, Ω_{nm} — the Stevens spin operators, b_{nm}, c_{nm} — the fine structure parameters. The numbers of the energy levels, between which the observed transitions were occurred, have been identified taking into account the procedures described in the study [12]. The rms deviation of the calculated resonance frequencies of the transitions from the measured resonance frequencies of the transitions has been minimized (by octic complex matrix diagonalization) to obtain the SH parameters of Table 1. As usual, the **g**-tensor of the Fe^{3+} centers turned out to be almost isotropic.

The same Table shows the second-rank fine structure tensor parameters for the two Fe^{3+} centers in the local (main) coordinate systems XYZ, which become diagonal one with the maximum $|D \equiv b_{20}| > |b_{22}|$. The main axes were obtained by rotating the coordinate system in the procedure of searching the highest value of $|D \equiv b_{20}|$. We note that several local coordinate systems satisfy this criterion. The transition from the laboratory coordinate system into one of the system of the main axes was done by subsequently rotating (zyz) for the Euler angles: 31; 13; 35.4° for Fe^{3+}-1 and 246; 65.3; 295.3° for Fe^{3+}-2. At the same time, the minimum angles between the main Z axes of these tensors and the **z** axis of the laboratory coordinate system are as follows: $\sim 13°$ for Fe^{3+}-1 and $\sim 65°$ for Fe^{3+}-2. The multiple local systems are due to existence of the two positions coupled by the C_2 || **b** operation, for the

Table 1. SH parameters of the two Fe^{3+} centers in Y_2SiO_5 in the **z** || **b** coordinate system and in the main axes of the second-rank fine structure tensor. (Double signs of b_{nm}, c_{nm} with the odd m correspond to the two centers coupled by the C_2 || **b** operation. Absolute signs of the parameters were not defined. b_{nm}, c_{nm} and the rms deviation F(N) are given in MHz, N — the number of the experimental values used in the optimization procedure, zero-field splitting (ZFS) — in GHz)

Parameters	Fe^{3+}-1 **z** || **b**	Fe^{3+}-1 in the main axes	Fe^{3+}-2 **z** || **b**	Fe^{3+}-2 in the main axes
g_x	2.041		2.043	
g_y	2.018		2.019	
g_z	2.010		2.010	
b_{20}	−5746	−6239	−1915	5936
b_{21}	∓6792	0	∓3409	0
b_{22}	−1823	2412	−4010	1897
c_{21}	∓5291	0	∓14263	0
c_{22}	1303	0	5338	0
b_{40}	−65	–	15	–
b_{41}	±170	–	∓317	–
b_{42}	−15	–	162	–
b_{43}	∓153	–	±30	–
b_{44}	4	–	322	–
c_{41}	∓116	–	∓214	–
c_{42}	80	–	134	–
c_{43}	±91	–	∓331	–
c_{44}	642	–	−92	–
F(N)	20.4 (903)		11.9 (418)	
ZFS	24.4 and 14.1		13.3 and 23.1	

Table 2. Ratio of the concentrations of the Fe^{3+}, Cr^{3+}, Gd^{3+} centers with the numbers 1 and 2 in the Y_2SiO_5 and Sc_2SiO_5 crystals. (The centers are designated as per the studies [2,8,12,13], the round brackets hold full initial splitting of the respective center and the minimum angle between its main axis and the **z** axis)

Crystal	Centers		Ratio of concentrations of centers 1/2
Y_2SiO_5	Fe^{3+}-1 (ZFS = 38 GHz, $\lambda = 13°$) this study	Fe^{3+}-2 (ZFS = 36 GHz, $\lambda = 65°$) this study	500
	Cr I (53, 51°) [8]	Cr II (52, 30°) [8]	700
	Gd1 (25, 66°) [12]	Gd2 (40, 19°) [12]	1
Sc_2SiO_5	Fe1 (46, 45°) [2]	Fe2 (59, 75°) [2]	1
	Cr1 (67, 54°) [13]	Cr2 (43, 68°) [13]	10
	–	Gd (47, 22°) [2,13]	–

yttrium ion. Besides, the relationship $|\mathbf{b}_{20}| > |\mathbf{b}_{22}|$ is also satisfied by the coordinate systems rotated around Z of the above-said system for the angles 90 and 180°, and around X and Y for 180°. The fourth-rank tensor was not analyzed due to high error of its components that demonstrated obvious instability in the optimization procedure.

The study [2] has cautiously assumed that the minimum angles (λ) between the main Z axes of the second-rank fine structure for the Fe^{3+}, Cr^{3+}, Gd^{3+} centers and the **z** axis of the laboratory coordinate system could be a criterion for determining localization of the impurity centers in the $M1$ or $M2$ sites. In addition to the above-noted angles between Z**z**, Table 2 also shows the ratio of the concentrations of the Fe^{3+}, Cr^{3+}, Gd^{3+} centers, which are localized in the $M1$ and $M2$ sites of yttrium and scandium silicates, as obtained by evaluating the integral intensities of the EPR signals with taking into account the probabilities of the transitions, as well as full zero-field splitting for this center. At the same time, it is necessary to take into account that the values of the components of the SH second-rank tensor and its main axes are determined by a rhombic part of the crystal field, which strongly depends on relaxation of the impurity ion environment.

The Fe^{3+}-1 and Cr I centers that demonstrate a high concentration in Y_2SiO_5 and have small ionic radii ($R_i = 0.55$ and 0.615 Å [18]) definitely occupy the position Y^{3+} in $M1$ with the coordination number 6 ($R_i = 0.90$ Å). In the similar position of scandium silicate (0.745 Å [18]), high concentration of the Cr1 center should also be expected.

The big Gd^{3+} ion having the 1 Å ionic radius in the seventh-fold environment obviously occupies a more spacious scandium position $M2$ in Sc_2SiO_5 (the average distance to the ligands is 0.88 Å). It is difficult to say something certain about localization of the Gd1 and Gd2 centers in Y_2SiO_5 and the Fe1 and Fe2 centers in Sc_2SiO_5, which have comparable concentrations.

4. Cu^{2+} centers

In an arbitrary orientation of the magnetic field, the EPR spectrum of the studied Y_2SiO_5:Fe sample has up to ~ 14 signals from each of the Gd1 and Gd2 centers, and ~ 10 lines, from each of the Fe^{3+}-1 and Fe^{3+}-2 centers. Besides them one can see multiple weak signals, and it is still impossible to identify many of them. At the same time, we have succeed to surely identify weak signals of the centers of the copper accidental impurity among them, although the presence of a large number of other signals made it difficult to obtain data about the orientation behavior of the positions of the weak signals of the Cu^{2+} centers.

Figure 6 shows the hyperfine quartets of the EPR spectrum of the copper center with the isotopes $^{63}Cu^{2+}$ ($S = 1/2$, the nuclear spin $I = 3/2$, the natural abundance 69%) and $^{65}Cu^{2+}$ ($S = 1/2$, $I = 3/2$, 31%), as detected by us in Y_2SiO_5. The similar quartets of noticeably smaller intensity are also seen in the Figure. Figure 1 can not show all the copper signals due to their small ($\sim 10^{-3}$) intensity in relation of the surrounding lines of the Gd1, Gd2 and Fe^{3+}-1 centers.

The polar and azimuth dependences of the positions of the hyperfine structure components of the copper centers are shown on Figures 7–8. The spectra of the two copper centers and their orientation behavior were described by means of the triclinic spin Hamiltonian

$$H_{sp} = \beta(\mathbf{BgS}) + \mathbf{SAI} + g_N\beta_N\mathbf{BI},$$

where **g** — the electron **g**-tensor, **A** — the hyperfine interaction tensor, β — the Bohr magneton. The calculations used tabular values of nuclear g_N-factors of the copper isotopes (β_N — the nuclear magneton), the nuclear quadrupole interaction was not taken into account because of its smallness. The SH parameters of the $^{63}Cu^{2+}$ and $^{65}Cu^{2+}$ centers were optimized by minimizing the rms deviation of the calculated resonance frequencies F of the

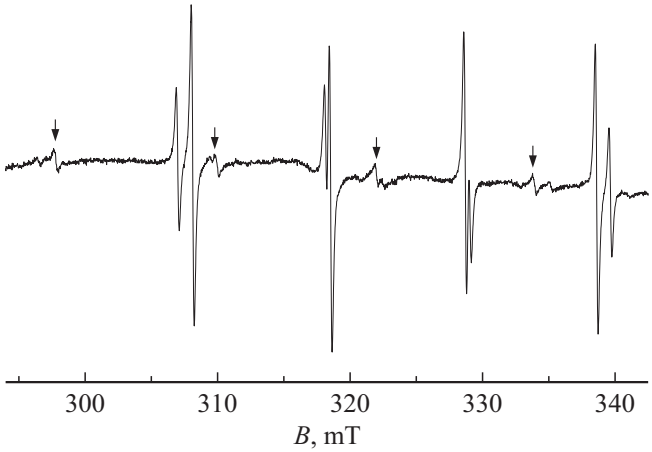

Figure 6. EPR-spectrum of the $^{63}Cu^{2+}$ and $^{65}Cu^{2+}$ centers (intense signals) in Y_2SiO_5 at $\theta = 90°$ and $\varphi = 180°$. The arrows mark the hyperfine structure transitions of the unstudied $^{63}Cu^{2+}$ centers.

transitions from the measured resonance frequencies of the transitions (by octic complex matrix diagonalization $\{2S + 1\} \times \{2I + 1\}$).

An attempt of describing the angular dependences of Figures 7–8 by the **g**- and **A**-tensors of a diagonal kind has resulted in the value of F about three hundred MHz, which in no way corresponded to the error in measurement of the signal position. In this regard, the repeated optimization procedure has used the **g**- and **A**-tensors of the general kind, since there are no limitations on the structure of **g** and **A** for the triclinic symmetry centers, in not the main axes, especially [19–22]. The optimization results are shown in Table 3.

Only when all the listed components of the **g** and **A** tensors were available, it was possible to describe the experimental dependences of the hyperfine structure positions quite well. It is indicated by the fact that taking into account only a symmetrical part of the **A**-tensor, the rms deviation F increases to 72 MHz (see Table 3).

The same table shows the SH parameters obtained by diagonalization of the $\mathbf{g}^2$ and $\mathbf{A}^2$ tensors [19–20]. The direction cosine matrices coupling the laboratory coordinate system and the systems of the main axes have turned out almost identical for the two isotopes to have values as follows: for the **g**-tensor

$$\begin{pmatrix} 0.672 & -0.122 & 0.731 \\ -0.458 & -0.844 & 0.280 \\ -0.582 & 0.523 & 0.623 \end{pmatrix},$$

for the A-tensors of $^{63}Cu^{2+}$ and $^{65}Cu^{2+}$

$$\begin{pmatrix} -0.754 & -0.128 & 0.645 \\ 0.493 & -0.759 & 0.426 \\ 0.435 & 0.639 & 0.635 \end{pmatrix}.$$

It has been later found that when using different starting values of A_{ij}, the optimization procedure (the components g_{ij} for $^{63}Cu^{2+}$ were taken from Table 3 without being varied) provided substantially different sets of A_{ij}, but with the minimum values of F (≈ 2 MHz). Two examples of these sets of A_{ij} for $^{63}Cu^{2+}$ can be seen in Table 4, which also contains the diagonalization results of $\mathbf{A}^2$ with the similar direction cosine matrices.

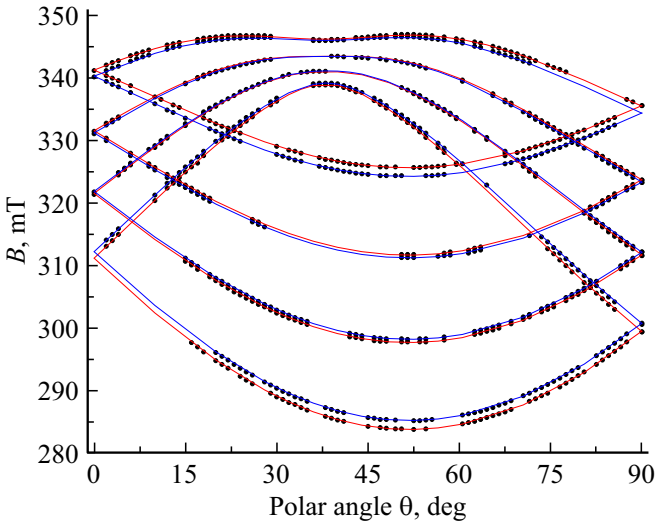

Figure 7. Polar angular dependence of the components of the hyperfine structure of the $^{63}Cu^{2+}$ and $^{65}Cu^{2+}$ centers in Y_2SiO_5 at $\varphi = 23°$. The dots — the experiment, the curves — calculation with the parameters of Table 3: the blue dashed ones — $^{63}Cu^{2+}$, the red solid ones — $^{65}Cu^{2+}$. A group of the signals that demonstrate the minimums of the positions belongs to the centers that are coupled to the others by the $C_2 \parallel \mathbf{b}$ operation. The sections of the calculated dependences without experimental dots appear due to overlapping of the copper signals by the intense lines of the other centers.

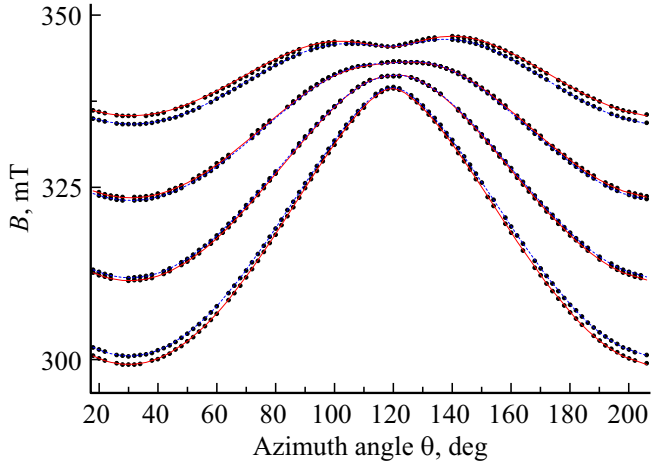

Figure 8. Azimuth angular dependence of the components of the hyperfine structure of the $^{63}Cu^{2+}$ and $^{65}Cu^{2+}$ centers in Y_2SiO_5. The dots — the experiment, the curves — calculation with the parameters of Table 3: the blue dashed ones — $^{63}Cu^{2+}$, the red solid ones — $^{65}Cu^{2+}$.

Table 3. Parameters of the spin Hamiltonian for the $^{63}Cu^{2+}$ and $^{65}Cu^{2+}$ centers in Y_2SiO_5. (The double signs correspond to the centers coupled by the $C_2 \parallel \mathbf{b}$ operation. The values of the A tensor components and the rms deviation F(N) are given in MHz, N — the number of the experimental values used in the optimization procedure)

Parameters	$^{63}Cu^{2+}$ $\mathbf{z} \parallel \mathbf{b}$	$^{63}Cu^{2+}$ in the main axes	$^{65}Cu^{2+}$ $\mathbf{z} \parallel \mathbf{b}$	$^{65}Cu^{2+}$ in the main axes
g_{xx}	2.151	2.000	2.151	2.000
g_{xy}	0.14		0.14	
g_{xz}	$\pm$0.23		$\pm$0.24	
g_{yx}	0.01		0.01	
g_{yy}	2.09	2.092	2.09	2.092
g_{yz}	$\mp$0.04		$\pm$0.04	
g_{zx}	$\pm$0.03		$\pm$0.03	
g_{zy}	$\pm$0.07		$\pm$0.07	
g_{zz}	2.145	2.302	2.145	2.302
A_{xx}	-187	28.2	-217	16.3
A_{xy}	-198		-196	
A_{xz}	$\mp$3.5		$\mp$10	
A_{yx}	-167		-173	
A_{yy}	-90	81.2	-99	85.3
A_{yz}	$\pm$12.7		$\pm$31.2	
A_{zx}	$\mp$162		$\mp$195	
A_{zy}	$\mp$208		$\mp$203	
A_{zz}	-69	421.0	-78	451.7
F(N)	2 MHz (500)		2.6 MHz (500)	

Most likely, the effect of ambiguity of the SH parameters is caused by deficiency of the experimental data, for example, absence of the positions of prohibited hyperfine transitions with $\Delta m_I \neq 0$, which can not be detected at such concentrations of the copper impurity.

The noticeable difference in the charges of the Cu^{2+} and Si^{4+} ions and in their ionic radii (0.57 and 0.26 Å [18] in the tetrahedron, respectively) makes it very unlikely that the copper ion will enter the silicon positions. In the six-fold environment, Cu^{2+} has the ionic radius of 0.73 Å, which is much more favorable for its localization in the *M1* Y^{3+} site (0.9 Å [18]) in terms of the difference both in the ionic radii and in the formal charges. It should be noted that the minimum angles between the main Z axes of the **g**-, **A**-tensors and the **z** axis of the laboratory coordinate system (51.5°, 50.6°) differ by $\sim 1°$ only. These angles well agree with the same angle of Table 2 for Cr I in the Y_2SiO_5 crystal, thereby supporting our assumption about localization of the copper ion. The charge can be compensated both locally and remotely.

We also note that besides the two quartets of the isotopes Cu^{2+} Figure 6 also exhibits a weak (with intensity smaller by an order of value) groups of the signals, which obviously belongs to another Cu^{2+} center. These signals may be due to the Cu^{2+} ions in the position *M1* with alternative compensation of the charge, or to the copper ions in the position *M2*. We have failed to measure the angular dependences of the positions of these very low-intensity signals in a dense spectrum of Y_2SiO_5 and, consequently, to measure the SH parameters therefor.

Table 4. Two sets of the components of the **A** tensors, as obtained for $^{63}Cu^{2+}$, in the laboratory coordinate system and in the main axes. g_{ij} components of Table 3

Parameters	First set		Second set	
	$\mathbf{z} \parallel \mathbf{b}$	in the main axes	$\mathbf{z} \parallel \mathbf{b}$	in the main axes
A_{xx}	-240	24	-208	47
A_{xy}	-129	0	-176	0
A_{xz}	-3	0	-3	0
A_{yx}	-130	0	-96	0
A_{yy}	-137	82	-164	72
A_{yz}	12	0	12	0
A_{zx}	-248	0	-187	0
A_{zy}	-95	0	-180	0
A_{zz}	-62	421	-82	421
F(N)	2 MHz		1.9 MHz	

5. Conclusion

Using the Czochralski method, the iron-doped yttrium orthosilicate single crystal has been grown. This sample was subjected to two-plane measurement of orientation behavior of the positions of the EPR signals of the two triclinic Fe^{3+} centers localized in the two non-equivalent positions of yttrium ions. The transitions of these centers were identified. Via minimizing the difference of the experimental and calculated frequencies of the transitions, the parameters

of their triclinic spin Hamiltonians were determined in the laboratory coordinate system.

The systems of the main axes of the second-rank fine structure tensors were found, wherein the parameters b_{20} had the maxima, and the **D** tensors became diagonal ones. Using the values of the angles between the main axis and the **z** axis, the ratio of the concentrations, the zero-field splitting values and the ionic radii of the pairs of the Fe^{3+}, Cr^{3+}, Gd^{3+} centers, it has been attempted to determine localization of these impurities in the yttrium and scandium silicates.

The same crystal has exhibited the weak EPR signals of the uncontrolled Cu^{2+} impurity. The polar and azimuth angular dependences of the positions of the components of the hyperfine structure of the $^{63}Cu^{2+}$ and $^{65}Cu^{2+}$ isotopes have been measured, all the components of the asymmetric **g** and **A** tensors have been determined. It has been shown that it is impossible to describe the angular dependences by the symmetric **A** tensor with accuracy comparable with the error of measurement of the positions of the transitions.

The study has found the direction cosine matrices, which couple the laboratory coordinate system and the systems of the main axes of $\mathbf{g}^2$ and $\mathbf{A}^2$, in which these tensors become diagonal ones. It is assumed that the copper ion occupies the *M1* Y^{3+} site with the six-fold oxygen environment, while the charge can be compensated both locally and remotely. The study has also detected the signals of another Cu^{2+} center (weaker by an order) that may be caused by the Cu^{2+} ions in the *M1* position with alternative compensation of the charge or by the copper ions in the *M2* position.

Funding

The study was financially supported by the Ministry of Science and Higher Education of the Russian Federation, topic No. FEUZ-2023-0017 using the equipment provided by Ural Common Use Center „Modern Nanotechnologies“ Ural Federal University (Reg. No. 2968).

Conflict of interest

The authors declare that they have no conflict of interest.

References

[1] D.D. Kramushchenko, I.V. Il'in, V.A. Soltamov, P.G. Baranov, V.P. Kalinushkin, M.I. Studenikin, V.P. Danilov, N.N. Il'ichev, P.V. Shapkin. FTT **55**, 234 (2013). (in Russian).
[2] V.A. Vazhenin, A.P. Potapov, K.A. Subbotin, A.V. Fokin, M.Yu. Artemov, A.I. Titov, S.K. Pavlov. FTT **65**, 773 (2023). (in Russian).
[3] B.H.T. Chai, Y. Simony, C. Deka, X.X. Zhang, E. Munin, M. Bass. OSA Proc. ASSL **13**, 28 (1992).
[4] Chih-Kang Chang, Jih-Yuan Chang, Yen-Kuang Kuo. Proc. SPIE **4914**, 498 (2002).
[5] R.R. Rakhimov, H.D. Horton, D.E. Jones, G.B. Loutts, H.R. Ries. Chem. Phys. Lett. **319**, 639 (2000).
[6] V.A. Vazhenin, A.P. Potapov, G.S. Shakurov, A.V. Fokin, M.Yu. Artemov, V.A. Isaev. FTT **60**, 1995 (2018). (in Russian).
[7] V.F. Tarasov, I.V. Yatsyk, R.F. Likerov, A.V. Shestakov, R.M. Eremina, Y.D. Zavartsev, S.A. Kutovoi. Opt. Mater. **105**, 109913 (2020).
[8] V. Vazhenin, A. Potapov, K. Subbotin, D. Lis, M. Artyomov, V. Sanina, E. Chernova, A. Fokin. Opt. Mater. **117**, 111107 (2021).
[9] A.P. Potapov, V.A. Vazhenin, M.Yu. Artyomov, G.S. Shakurov, R.B. Zaripov, K.A. Subbotin, A.V. Shestakov. Opt. Mater. **143**, 114149 (2023).
[10] V. Tarasov, R. Eremina, K. Konov, R. Likerov, A. Shestakov, Y. Zavartsev, S. Kutovoi. Appl. Magn. Res. **52**, 5 (2021).
[11] A.A. Sukhanov, V.F. Tarasov, R.M. Eremina, I.V. Yatsyk, R.F. Likerov, A. V. Shestakov, Y.D. Zavartsev, A.I. Zagumennyi, S.A. Kutovoi. Appl. Magn. Res. **52**, 1175 (2021).
[12] A.V. Fokin, V.A. Vazhenin, A.P. Potapov, M.Yu. Artyomov, K.A. Subbotin, A.I. Titov. Opt. Mater. **132**, 112741 (2022).
[13] V.A. Vazhenin, A.P. Potapov, A.V. Fokin, M.Yu. Artemov, V.A. Isaev. FTT **64**, 967 (2022). (in Russian).
[14] B.A Maksimov, V.V. Ilyukhin, Yu.A. Kharitonov, N.V. Belov. Kristallografiya **15**, 926 (1970). (in Russian).
[15] G. Anan'eva, A. Korovkin, T. Merkulyaeva, A. Morozova, M. Petrov, I. Savinova, V. Startsev, P. Feofilov. Inorg. Mater. **17**, 754 (1981).
[16] N.I. Leonyuk, E.L. Belokoneva, G. Bocelli, L. Righi, E.V. Shvanskii, R.V. Henrykhson, N.V. Kulman, D.E. Kozhbakhteeva. Cryst. Res. Technol. **34**, 1175 (1999).
[17] S.A. Altshuler, B.M. Kozyrev. Elektronnyi paramagnitnyi rezonans soedineniy elementov promezhutochnykh grupp. Nauka, M., (1972). S. 121. (in Russian).
[18] R.D. Shannon. Acta Crystallogr. Sect. A: Cryst. Phys., Diffr., Theor. Gen. Crystallogr. **32**, 751 (1976).
[19] Zh. Verts, J. Bolton. Teoriya i prakticheskie prilozheniya metoda EPR. Mir, M. (1975), 548 p. (in Russian).
[20] A. Abragam, B. Blini. Elektronnyj paramagnitnyj rezonans perekhodnykh ionov. Mir, M. (1973). T. 2. 347 p. (in Russian).
[21] F.K. Kneubühl. Helv. Phys. Acta. **35**, 259 (1962).
[22] F.S. Ham. J. Phys. Chem. Solid **24**, 1165 (1963).

Translated by M.Shevelev